IEEE Access
Multidisciplinary ⋮ Rapid Review ⋮ Open Access Journal

Received December 2, 2020, accepted January 6, 2021, date of publication January 8, 2021, date of current version January 15, 2021.

Digital Object Identifier 10.1109/ACCESS.2021.3050243

ANN Assisted Multi Sensor Information Fusion for BLDC Motor Fault Diagnosis

TANVIR ALAM SHIFAT, (Graduate Student Member, IEEE), AND JANG-WOOK HUR
Department of Aeronautics, Mechanical, and Electronic Convergence Engineering, Kumoh National Institute of Technology, Gumi 39177, Republic of Korea
Corresponding author: Jang-Wook Hur (hhjw88@kumoh.ac.kr)

This work was supported by the Ministry of Science and ICT (MSIT), South Korea, through the Grand Information Technology Research Center Support Program supervised by the Institute for Information & Communications Technology Planning & Evaluation (IITP) under Grant IITP-2020-2020-0-01612.

ABSTRACT Multiple sensor data fusion is necessary for effective condition monitoring as the electric machines operate in a wide range of diverse operations. This study investigates sensor acquired vibration and current signals to establish a reliable multi-fault diagnosis framework of a brushless DC (BLDC) motor. Faults in stator and rotor were created deliberately by shorting two adjacent windings and creating a hole on the surface, respectively. The threshold for different health states was obtained by the third harmonic analysis of motor current. Later, the key features from sensor acquired current and vibration signals are selected based on monotonicity and reduced using the principal component analysis (PCA). For future predictions, an artificial neural network (ANN) is used to classify different fault features and its performance is evaluated using several metrics. Analysis of motor current harmonics and impulsive vibration response at the same time provides a thorough health estimation of BLDC motor in the presence of both electrical and mechanical faults. Multiple sensor information is fused to obtain a better understanding of the fault characteristics and mitigate the randomness of fault diagnosis. The proposed model was able to detect and classify multiple fault features with higher accuracy compared to other similar methods.

INDEX TERMS ANN, BLDC motor, condition monitoring, CEEMD, fault diagnosis.

I. INTRODUCTION

Predictive maintenance (PdM) using data-driven approaches has become quite popular in academia and industries. The major advantage of a data-driven maintenance framework is that it does not require a prior physics of failure model of the system [1]. A proper mathematical model is often difficult to establish, and considering the intricate industrial operations, a physical model will require continuous updating based on operating conditions. This is a time consuming and economically expensive task. Therefore, data-driven methods have gained popularity over the model-based methods over the years. Also, ease in acquiring and storing big-data, availability of computational resources, advances signal processing techniques, etc. have made data-driven approaches on top of the maintenance frameworks [2]. In a PdM framework, there are mainly two challenges. One is the fault diagnosis and the other is fault prognostics. Prognostics is making predictions based on historical failure data. Therefore, fault diagnosis is the foremost important step in a PdM framework that should be implemented precisely [3].

An increase in the production demand has made the industrial machines to run in a complex operating condition. Depending on the variety of necessities, an electric machine runs in both stationary and nonstationary operating conditions. In case of rotary machinery operation, stationary refers to the fact that the machine is operating under fixed load and speed [4]. Electric motors are expected to deliver a fixed mechanical output given a fixed electrical input in a stationary condition. On the other hand, machinery operation with variable speed and loading conditions is referred to as nonstationary operation [5]. In case of a fault, due to the changes in operation parameters, the fault patterns also change with different operating conditions making it a difficult task to detect and isolate the fault. In literature, there are a plethora of methods available to detect and diagnose these faults [6]. However, most of them are based on the single sensor data and univariate methods. In this study, we propose a fault diagnosis framework of BLDC motor combining multiple sensor data for accurate fault detection and classification.

The associate editor coordinating the review of this manuscript and approving it for publication was Hao Luo.

Brushless DC motor (BLDC motor) is an improvement over the conventional brushed DC motors. The major advantage of BLDC motor is that it does not have a mechanical commutator unlike brushed DC motor. Lack of a mechanical part gives BLDC motor several other benefits such as- longer lifetime, noiseless operation, precise control, better speed-to-torque ratio, etc. High reliability is the defining characteristic of BLDC motor [7]. Nevertheless, like other electrical machines, a BLDC motor can also fail due to complex operations and overload. Since there is no mechanical part between the stator and rotor, the entire commutation in a BLDC motor is based on the electromagnetic induction between the stator and rotor. Stator is a winding of conductor coils that can carry different polarity currents through the wires creating temporary electromagnets. On the other hand, rotor is a permanent magnet in a BLDC motor. By switching the polarity of stator coils, permanent magnet is rotated by continuous attraction and repulsion of opposite and different poles, respectively. Therefore, a fault in the stator or rotor operation will significantly affect the entire motor operation and if not monitored properly, it can lead to catastrophic system failures [8]. To get a thorough intuition about the fault characteristics as well as establishing a total fault diagnosis framework, in this study, we have investigated both the stator and rotor related faults at the same time. Both faults are deliberately created in a BLDC motor. In stator, a winding short circuit is created by joining two adjacent stator coil windings and this fault is referred to as WSC fault. And, in rotor, a crack is created by producing a hole in the permanent magnet, which is referred to as CRF fault.

In literature, several methods are adopted by researchers to detect and diagnose electric motor faults. For example, Park *et al.* used input impedance as an early fault detection factor of a BLDC motor subjected to inter-turn fault [9]. The same authors also diagnosed BLDC motor eccentricity related faults using stator current spectral analysis [10]. Kar *et al.* monitored gearbox vibration through the motor current signature analysis (MCSA) [11]. Kia *et al.* used the current vector analysis for gear tooth surface fault detection [12]. Among them, harmonic analysis of motor current has been proven to be the most effective one for early fault diagnosis. Also, monitoring current spectra does not require any advanced signal processing technique and can be performed keeping the motor in operation. This allows an opportunity for online condition monitoring of BLDC motors.

In data-driven maintenance frameworks, several sensor-acquired data are processed and analyzed to investigate the diagnostic related information of a system. Depending on the system architecture, the data type can be varied from acoustic emission monitoring to magnetic flux induction monitoring. Vibration is the most used sensor-data for fault diagnosis and condition monitoring of rotary machinery [13]. There are two main reasons behind that:

(a) Easy to handle: Acquiring vibration data does not require any prior knowledge of the system. Mounting and acquiring vibration data using a sensor provides ease even in a complex environment [14].

(b) Easy to process: Fault in a rotating component can be easily diagnosed by analyzing the changes in frequency patterns. By using advanced signal processing techniques such as- time-frequency analysis, fault characteristics for an abruptly changing vibration response can also be detected. Also, the vibration response of a component lifetime can be monitored using a single sensor. This vast amount of data widens the opportunity of fault diagnosis and prognosis using machine learning techniques [15].

Faults in industrial operation are random in nature and multi-sensor data are required for a reliable condition monitoring framework. Based on the degree of stress on motor, its electrical and mechanical signatures can vary significantly [16]. For example, an electric motor exhibits abrupt vibration response and increased phase currents if a larger load is connected to it. This does not imply the motor has deviated from the healthy state. Monitoring multi-sensor data reduces the chance of having a false alarm about the fault in motor. However, combining multiple sensor data and building a reliable fault diagnosis framework is a challenging task as different sensor data will evolve differently. Another challenge in using multiple sensor data is that for a fault, one sensor data will show anomalous behavior but the other might not show a distinguishable change in trend. In this paper, we have taken these challenges into consideration and built a multi-sensor fault diagnosis framework for BLDC motor in the presence of two different faults.

In this study, we have acquired and investigated the motor vibration response to detect different faults at the early stage for both stationary and nonstationary operations. Vibration response shows reasonable fault patterns when the fault is at a severe stage. However, extracting fault characteristics at the incipient stage is a challenging task as the irregular frequency components are difficult to detect. To have a better intuition about the weak fault frequencies, we performed complete ensemble empirical mode decomposition (CEEMD) technique. CEEMD is an improvement over the empirical mode decomposition (EMD) introduced by Huang *et al.* [17]. CEEMD overcomes the mode-mixing problem of EMD method and minimizes reconstruction error produced in EEMD method [18]. After the selection of proper IMF, several features are extracted from the IMF that play the role of health indicator (HI) in maintenance field. We have considered HI extraction from time domain and frequency domain, both to have a wide range of diagnostic information. On the other hand, harmonic signature analysis is performed on motor current signals to detect winding short-circuit faults. Zero sequence components also referred to as the third harmonics of motor current is an indication of fault [19]. To diagnose motor faults, third harmonic magnitude and frequency is computed and later, fault features are extracted from the sensor signal.

HIs from three different health states namely, healthy state, WSC fault state, and CRF fault state are classified using an

artificial neural network (ANN) [20]. Due to the abundance of big data and excellent performance, ANN is a widely used method in the machinery fault diagnosis. HIs hold different patterns for different health states which can be compared to the pattern recognition problem in the deep learning field [21]. Some of the applications of ANN in condition monitoring field are electrical load forecasting [22], fault diagnosis of rolling element bearings [23], transformer fault diagnosis [24], bearing fault diagnosis [25], etc. Another feature of ANN is its simple architectural design. It basically consists of one input layer, one output layer, and one or more hidden layers. However, the selection of hyperparameters is a challenging task as the model might get overfitted or underfitted. In this study, model parameters of ANN are done by several trial-and-error bases. After training the neural network, its performance was tested and several performance metrics are computed, and model performance is evaluated based on those metrics. The goals of this study are:

(a) Decision making based on multi-sensor data.
(b) Create a feature set by preserving the multi-sensor fault characteristics.
(c) Fault classification using a neural network approach.

The main goal of this study is to establish a multi-fault diagnosis framework using multiple sensor information which can be further used for different stator and rotor related faults of BLDC motor.

II. PROPOSED METHOD

In this study, we propose a robust fault diagnosis framework based on multi-sensor data fusion that will detect and classify BLDC motor faults at the incipient stage. Main aim of this paper is early fault detection of BLDC motor for both mechanical and electrical faults at the same time. A crack is made on the rotor body to produce a mechanical fault and two adjacent windings are shorted together to produce an electrical fault. Motor current is used to FDI of a stator related fault named winding short-circuit (WSC). And vibration signals are analyzed to detect rotor related fault called crack rotor fault (CRF). Third harmonics of motor currents are analyzed to detect irregularity in the stator coil operation. Frequencies of these harmonics as well as the amplitude are also determined to understand the fault magnitude. For the vibration signals, signals are decomposed into IMFs using CEEMD technique. CEEMD allows us to find the hidden fault characteristics which is a difficult task to find by directly analyzing the raw vibration signals. After CEEMD decomposition, several features are extracted from the best-fit IMF in time-domain and frequency-domain. Primary concern of this study is to merge mechanical and electrical fault features by combining fault characteristics from vibration and current signals, respectively. Most appropriate features from the current and vibration signals are chosen based on the monotonicity score. Selected features are further reduced to a 2-D feature space using the principal component analysis (PCA) method. A combination of monotonicity score and PCA allows us to efficiently classify the fault states by preserving the dominating fault characteristics of both sensor signals. A concise framework of the proposed method is shown in Fig. 1.

III. RELATED THEORIES

A. COMPLETE ENSEMBLE EMPIRICAL MODE DECOMPOSITION

EMD is an adaptive signal processing technique that can decompose a time series signal into corresponding orthogonal components called IMFs. It is a popular technique to observe the hidden characteristics of a signal by decomposing it into some mode functions and residuals. In EMD, a signal is decomposed into corresponding intrinsic mode function (IMF) and residual each having different characteristics. One major drawback of EMD technique is that mode aliasing problem. That is the mix of frequency components into different IMFs. In the field of fault diagnosis, this can lead to erroneous approximation as we need to detect the fault frequencies from sensor data. As mentioned earlier, EEMD is introduced to improve the move aliasing phenomena in EMD by adding Gaussian white noise to the original signal [26]. However, during the reconstruction, removal of this noise leads to a larger computational time and reconstruction error. To overcome these issues, a better decomposition method, CEEMD is proposed which works with adaptive noise. Both techniques work on a similar basis called sifting process. CEEMD overcomes the mode-mixing problem with almost zero reconstruction error [27]. Major steps of a sifting process are:

Step 1: Identification of all local minima and maxima points of the signal x(t).

Step 2: Find the upper envelope, $e_u(t)$ and the lower envelope, $e_l(t)$.

Step 3: Calculate the mean envelope:

$$m(t) = \frac{e_u(t) - e_l(t)}{2} \tag{1}$$

Step 4: Obtain the primitive value of IMF as:

$$h_k(t) = h_{k-l}(t) - m_{k-l}(t) \tag{2}$$

Step 5: Store $h_k(t)$ as an $IMF_i(t)$ if it satisfies all the conditions of an IMF.

Step 6: Compute residuals as:

$$r_i(t) = x_i(t) - IMF_i(t) \tag{3}$$

In step 5, the conditions of considering the output as IMF are:

(a) The discrepancy between the number of extrema and the number of zero-crossings must be either equal or differ at most by one.
(b) At any point, the mean value of the IMF is zero.

In CEEMD, IMF is obtained by adding a white noise at each stage of the IMF computation [28]. ε_i denotes the noise coefficient at the i^{th} level of decomposition where $i = 1, 2, 3 \ldots\ldots N$. The first IMF is computed same as the EEMD

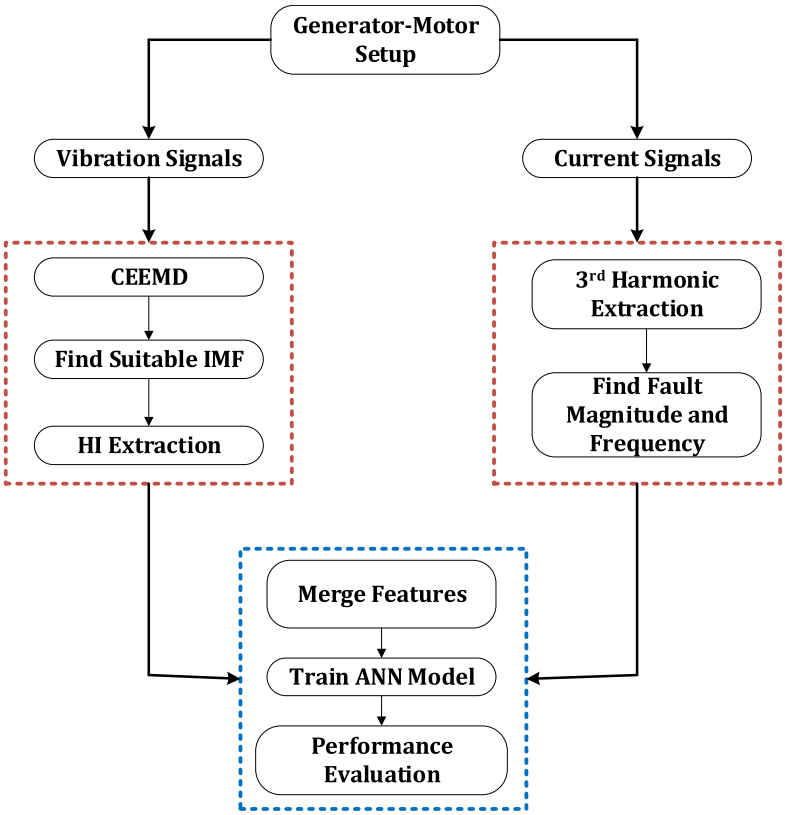

FIGURE 1. Proposed fault diagnosis architecture.

method and the residual of the first computation is shown in (4).

$$\widetilde{IMF}_1(t) = \frac{1}{I}\sum_{i=1}^{I} IMF_{i1}(t) = \overline{IMF}_1(t) \tag{4}$$

$$r_1(t) = x(t) - \widetilde{IMF}_1(t) \tag{5}$$

Thus, the second IMF is computed as:

$$\widetilde{IMF}_2(t) = \frac{1}{I}\sum_{i=1}^{I} E_1(r_1(t) + \varepsilon_1 E_1(\omega_i(t))) \tag{6}$$

$$r_2(t) = r_1(t) - \widetilde{IMF}_2(t) \tag{7}$$

Here, $E_k[\blacksquare]$ operator defines the k^{th} mode defined by the EMD method. $\omega_i(t)$ is the adaptive white noise added in each stage of IMF computation. After the modes are computed and necessary stopping criteria are met, the final signal can be reconstructed using the following equation.

$$x(t) = \sum_{k=1}^{K} \widetilde{IMF}_k(t) + R_k(t) \tag{8}$$

B. ARTIFICIAL NEURAL NETWORKS

Ease in acquiring and handling big data has given neural networks a boost in the field of machinery health assessment. Compared to conventional machine learning algorithms, ANNs have better accuracy for large datasets [29]. The concept of the ANN was established by mimicking human brain operation where the neurons share information throughout the neural connection to make a decision. In ANN, there are several layers that are interconnected to map the input and output. Basically, there are three layers in an ANN architecture [30]. The first one is the input layer where the ANN takes input data. The second one is hidden layer. In hidden layer, input data is taken and processed by some weight computation. The third layer is the output layer, where the weighted data is mapped with target neurons for decision making. Internal weights can be optimized to better capture the implicit mapping of input-output data.

To solve a classification problem, a set of pairs of training data are fed into the ANN model. For a training set, $\{(x_1, y_1), (x_2, y_2), (x_3, y_3) \ldots\ldots\ldots (x_N, y_N)\}$, x_i denotes the feature and y_i denotes the label of i^{th} feature. The number of neurons in the input layer is equal to the number of features that are to be trained in the ANN model. Each neuron has a weight and the product of this weight and the input value is transferred to the next neuron as an output. An activation function is used to map the input values to the output of the next neuron. There is a plethora of activation functions available for neural networks each having certain characteristics. To train an ANN model, an effective and computationally efficient activation function should be chosen. In this study, rectified linear unit (ReLU) is used as activation function in the hidden layers and sigmoid is used in the output layer.

TABLE 1. Parameters for motor test.

Parameter	Value
Motor Model	BLS-24026N
Generator Model	BLS-24040N
Rated values	Power: 26W Speed: 4000RPM Current: 1.7A
DAQ System	National Instruments (NI cDAQ-9178)
DAQ Module [Vibration]	Vibration: NI 9234 Current: NI 9246 Temperature: NI 9214 Voltage: NI 9205
Input	Voltage: 24 V_{DC} Current: 7A (max)
Loads	10MΩ DELTA
Sampling Rate (Vibration)	Vibration: 25.6 kHz Current: 5 kHz
Stator Coil Temperature	40-50 °C

A major concern in designing an ANN framework is hyperparameter optimization. Selection of proper activation function, depth of the network, loss function, dropout rate, etc. largely influence the performance of the model [31]. These hyperparameters are chosen during the training stage and based on the performance of prediction, these can be optimized further. In a classification problem, several performance measures can be used to evaluate model accuracy. For example, precision, recall, F1-score, geometric mean, etc.

IV. EXPERIMENT DESCRIPTION

A. TEST RIG SETUP

A 2-pole 12 winding interior permanent magnet (IPM) type BLDC motor is used in this study. BLDC motor is coupled with a BLDC generator with the help of a mechanical coupling. Since there is no mechanical connection between the stator and rotor, the entire commutation of BLDC motor is done by means of electromagnetic induction between the stator and rotor. Stator is a winding of conditioner coils and rotor is a permanent magnet. Based on the pole position of rotor, opposite poles are created in the adjacent stator windings to attract the rotor's pole. Thus, the rotor tries to align with the stator pole position which is controlled externally by supplying a pulse width modulated (PWM) input. A motor driver is used to sense the rotor position and supply corresponding polarity current to the stator windings. An embedded hall effect sensor (HES) in the motor sense the rotor position, and the motor driver alters the line currents' polarity according to the HES signal. It is understandable that any irregularity in stator or rotor operation will disturb the normal operation of BLDC motor and affect the desired output. These anomalies can be detected by monitoring and analyzing motor current, vibration, stator coil temperature, generated output, etc.

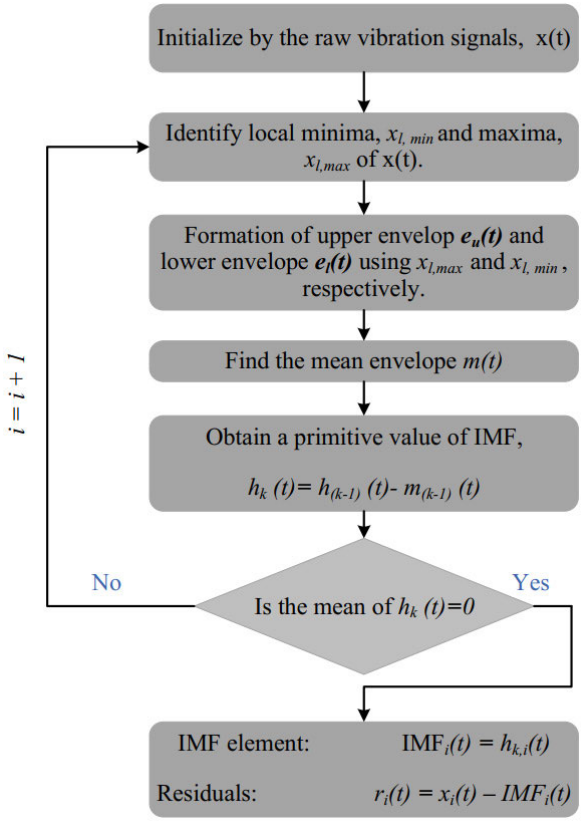

FIGURE 2. Sifting process for IMF computation in EMD.

In this study, we are mainly focused on motor vibration and current signals. Vibration signals are acquired using an integrated electronics piezotronics (IEPE) sensor mounted on top of it and the current signal for all three phases was acquired by using a direct line-to-line connection. A chassis NI cDAQ-9178 is used from national instruments (NI) with different embedded modules for different data acquisition. A brief description of the apparatus used in this study is presented in Table 1.

The test rig consists of a G-M setup where the motor is coupled with a generator through a mechanical coupling. A regulated constant power DC source is used to supply voltage to the motor driver. Motor driver then converts the DC into a PWM waveform and delivers it into the three-phase stator winding. Some external loads are connected to the generator end to create different levels of loadings. Vibration and current data are acquired continuously and stored in the hard-disk drive. A test bench photo is presented in Fig. 4 showing the sensors and DAQ setup.

B. FAULT DESCRIPTIONS

Several electrical and mechanical faults can take place in a BLDC motor. Some of the commonly occurring rotor faults are bent shaft, broken edge, misalignment, etc. Most of these faults directly or indirectly interrupt the magnetic field

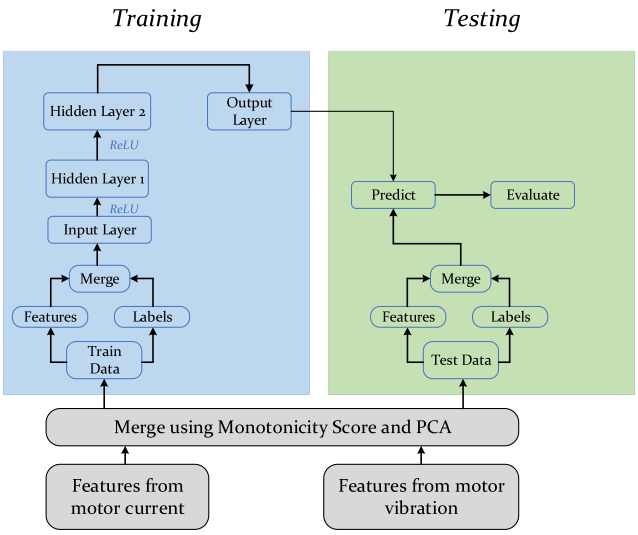

FIGURE 3. Proposed ANN architecture.

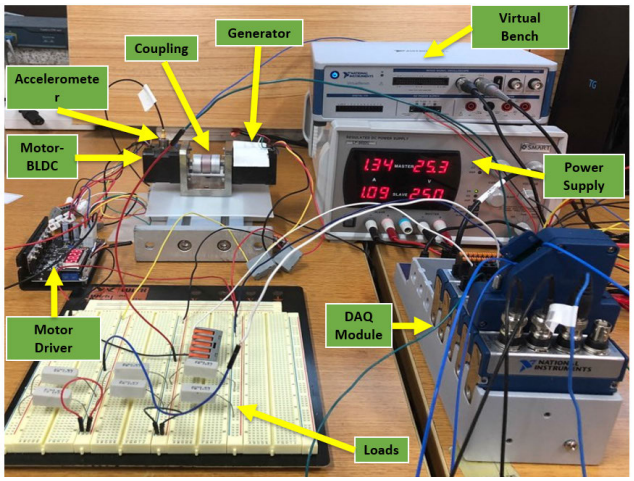

FIGURE 4. Test rig setup for motor test.

distribution of the permanent magnet, which causes imbalance in electromagnetic induction. Imbalanced induction produces several attributes in motor operation including abrupt vibration change, distorted phase currents, local heating, torque reduction, noise emission, etc. Primarily, mechanical faults are responsible for early vibration change and electrical faults produce inconsistent line currents [32].

In this study, we have investigated both the stator and rotor faults at the same time. A rotor fault is introduced by creating a circular crack with a diameter of 3.2 mm and depth 1.6mm. On the other hand, different types of short-circuits such as: inter-turn, coil-to-ground, coil-to-coil, etc. are the most frequent faults that take place in the stator. For stator fault, a winding short circuit is created by joining phase A and phase C. It should be noted that each four coil windings are connected internally to create a single phase in the stator part. Hence, there are three different phases each having four common coils connected together. All three phases are arranged in a star configuration having a common neutral node. During each step of commutation, two phases are energized with a positive and negative current where the

TABLE 2. BLDC motor commutation logic.

Step	Hall Sensor			Phases			Windings		
	H1	H2	H3	A	B	C	W_{AB}	W_{BC}	W_{AC}
I	1	0	1	+	0	N	-	N	N
II	0	0	1	+	N	0	N	N	+
III	0	1	1	N	+	0	N	-	N
IV	0	1	0	0	+	N	+	N	N
V	1	1	0	0	N	+	N	N	-
VI	1	0	0	N	0	+	N	+	N

third phase is kept unenergized. For example, in Fig. 5, phase A is energized with a negative polarity current and phase C is energized with a positive polarity current and phase B is kept neutral. On the next step commutation, phase current polarity is altered according to the pole position of rotor. A phase-winding commutation logic for BLDC motor is presented in Table 2. Due to this stepwise commutation, a fault in a BLDC motor leaves diagnostic information in its current and vibration signals. Our aim is to locate and isolate both types of faults by analyzing motor current and vibration signals.

V. RESULT ANALYSIS

A. FAULT DETECTION

As mentioned earlier, stator operation is the driving factor for a proper electromagnetic induction in BLDC motor operation since there is no mechanical commutator. Motor current signature carry significant diagnostic related information to detect and diagnose stator and rotor related faults in BLDC motors. MCSA can be done in various ways depending on the problem and solution. Such as- harmonic analysis, vector space analysis, wavelet analysis, etc. In this study, we chose to perform harmonic analysis as it is easy to compute and studies have shown it can diagnose different stator and rotor related faults efficiently [8], [19]. Harmonics are the multiplied fundamental frequency (f_n) components in a sinusoidal waveform. In an ideal case, a sinusoidal wave should consist of only one frequency, fn. However, due to the diverse and intricate operating conditions, different harmonics can be seen in real life signals. Harmonics in an electrical machine signal can be categorized into three class:

(a) Positive sequence: These harmonics are responsible for forward rotation.
(b) Negative sequence: These harmonics cause reverse rotation of synchronous direction causing the motor to slow down.
(c) Zero sequence: These harmonics do not disturb the rotation of motor, but, adds current to the neutral node of stator coils which causes excessive heating and distorted line currents.

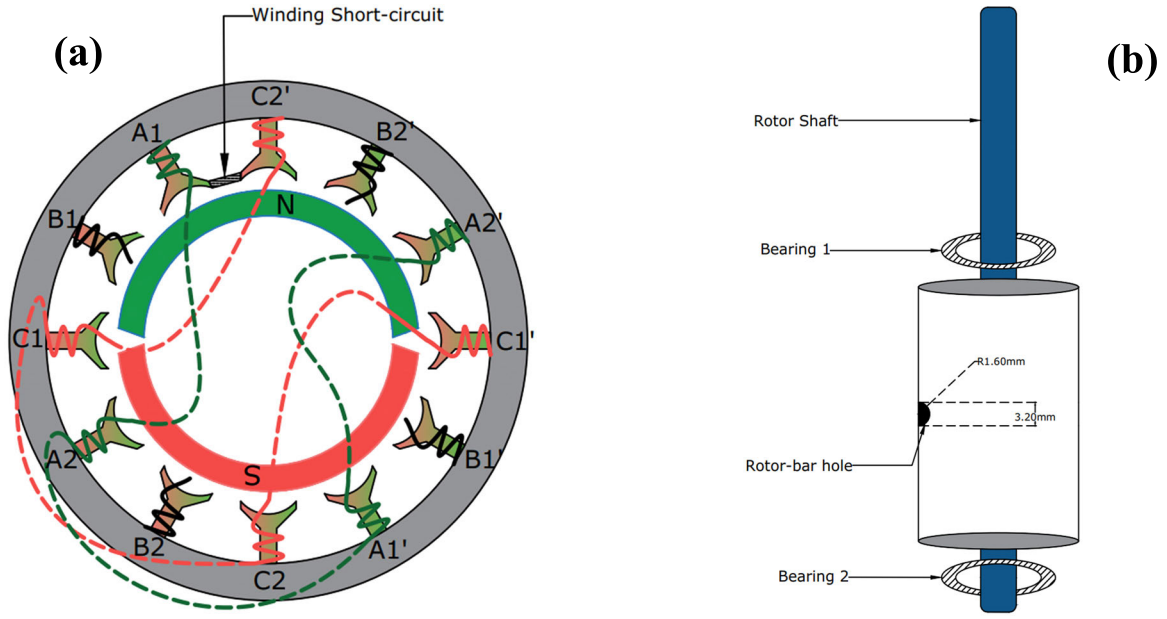

FIGURE 5. CAD illustration of motor faults. (a) Stator winding short-circuit (WSC). (b) Rotor crack fault (CRF).

Therefore, presence of third harmonics in the motor current spectra is considered as an irregular stator operation [35]. As the motor phases are organized in a Y-configuration, third harmonic indicates a current flow in the neutral junction of stator windings. This current initially produces excessive heating in the stator coils and gradually further irregularities in the stator operation. Also, as per the Kirchhoff's current law (KCL), the amount of current entering the node should be equal to the amount of current leaving that node. The presence of third harmonic component also indicates a violation of KCL [19]. In this study, we took this characteristic as a diagnostic feature to detect and localize the faults in BLDC motor for both, stator, and rotor faults. Motor current signals and harmonics are presented in Fig. 6. It can be seen that in healthy state operation, there is no visible third harmonics in current spectra. However, for WSC and CRF faults, the presence of third harmonics is observed which indicates an irregularity in motor operation. The fundamental frequency for the WSC fault signal is 300 Hz and the harmonics are located at 1.18 kHz and 2.36 kHz with a magnitude of 1.03 and 0.30, respectively. On the other hand, for CRF fault signal, third harmonics are found at 1.48 kHz and 2.28 kHz with a magnitude of 0.40 and 0.14, respectively. WSC fault directly affects the stator current operation and therefore the harmonic peaks are higher. In case of CRF fault, motor current is affected by the irregular magnetic flux distribution produced by the opposite magnetic pole in permanent magnet (rotor). Therefore, the effect of harmonic distortion is smaller compared to the WSC fault.

B. FEATURE EXTRACTION AND SELECTION

Motor vibration signals are decomposed using the CEEMD approach into five IMFs. Each IMF comprises unique fault patterns and shows distinguishable patterns which are difficult to detect using the sensor vibration signals. CEEMD decomposition of signals are shown in Fig. 7. Pearson correlation coefficient, ρ is computed to find the best fit IMF and compute features that serve the purpose of health indicators (HIs). Pearson correlation coefficient can be defined as (9). In case of healthy state signal, IMF-2 is selected as with highest correlation, $\rho = 0.82$ to the sensor signals. For faulty state signal, IMF-3 is selected which has $\rho = 0.86$. A portion of vibration signals with 10,000 samples are analyzed, and decomposition is shown in Fig. 7. Magnitude spectrums for the sampling frequency (25.6 kHz) are shown in the right column of each time-domain signals. In case of IMFs, frequency response of more centered to the fundamental frequency region making it easier to capture the diagnostics related information in the frequency domain.

$$r = \frac{\sum_i^n (x_i - \bar{x})(y_i - \bar{y})}{\sqrt{\sum_i^n (x_i - \bar{x})^2} \sqrt{\sum_i^n (y_i - \bar{y})^2}} \tag{9}$$

Several features are extracted from the motor current and vibration signals that serve the purpose of HI. Mathematical representation of the features and their physical significance for system condition monitoring are presented in Table 3. A further description of the features can be found in [33], [34]. Features, F1-F8 are extracted from the time domain signal whereas, F9-F12 are computed from the frequency domain. Same feature is extracted from the time domain and frequency domain since the goal of this study is to fuse multiple sensor data. A combination of multidomain HIs ensures a reliable and detailed health state estimation of motor.

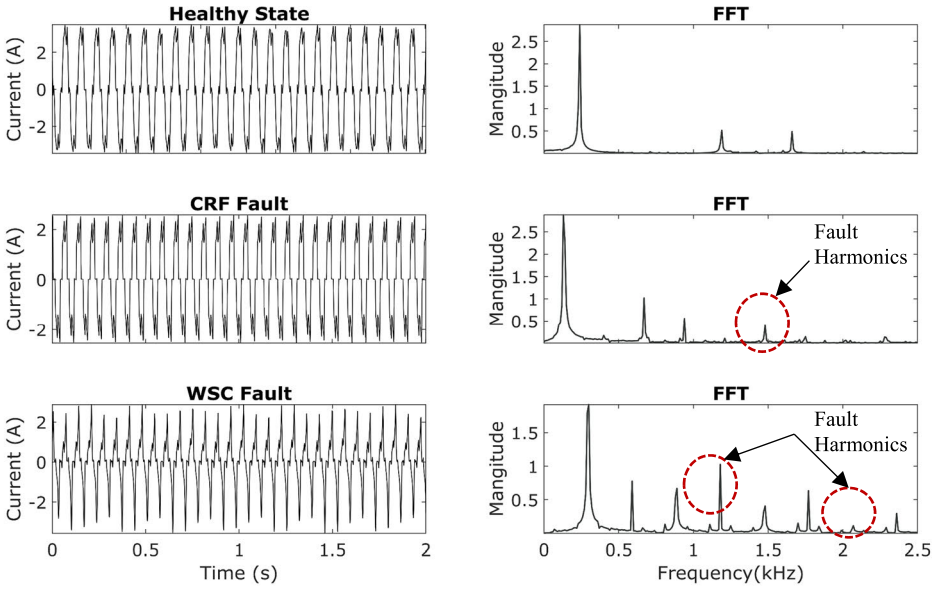

FIGURE 6. Motor current signature analysis.

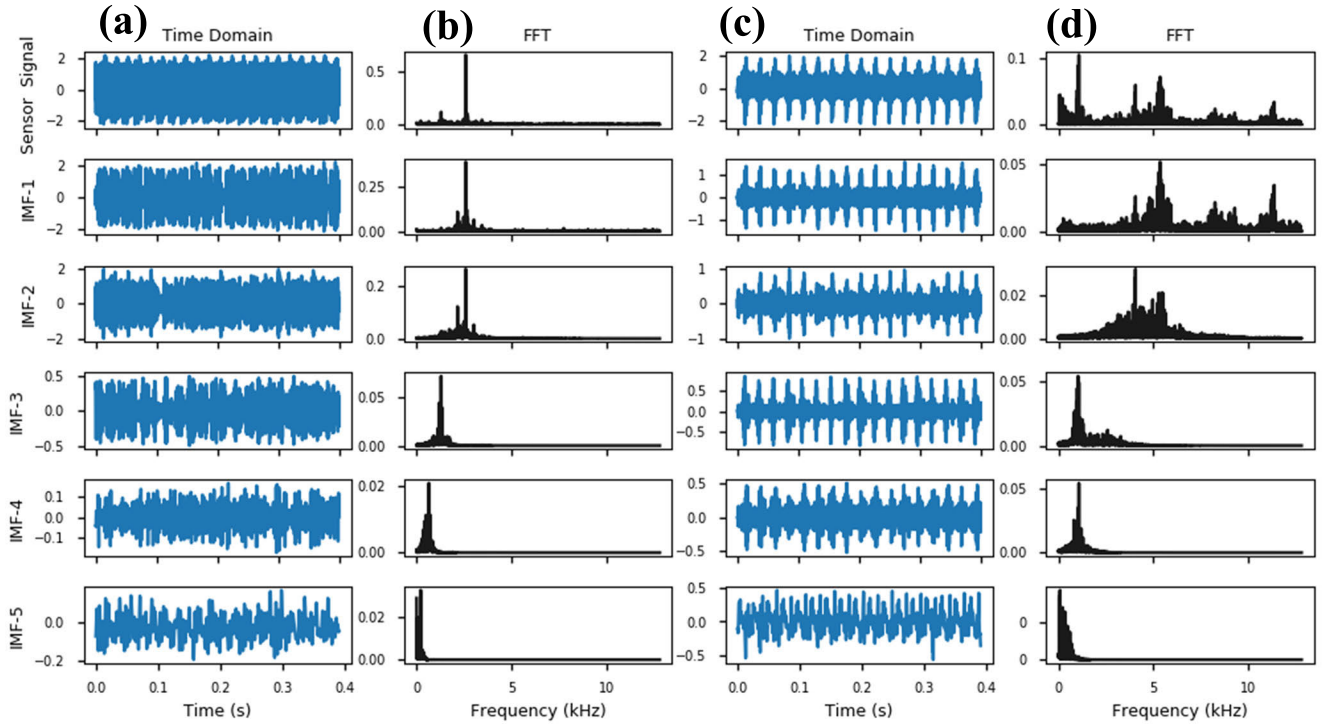

FIGURE 7. CEEMD decomposition of vibration signals. (a) Healthy signal and IMFs, (b) FFT of the healthy signal and IMFs, (c) Faulty signal and IMFs, (d) FFT of the faulty signal and IMFs.

C. FAULT CLASSIFICATION

We have used a monotonicity test to quantify the fault patterns between HIs extracted from current and vibration signals. Monotonic score is ranged from 0 to 1 where 0 indicates the feature is non-monotonic and 1 indicates the feature is perfectly monotonic [36]. Monotonic score can be defined as (10) where dF is the differential of feature series and T is the length of features. A higher monotonic score indicates the fact that it will show distinguishable diagnostic characteristic to classify the faulty states accurately. The monotonicity scores of current and vibration features are shown in Fig. 8. A feature having a higher monotonic value is considered to select the corresponding feature set. For example, for F1 feature, vibration shows a better monotonic trend compared to current. So,

TABLE 3. Features computed from vibration and current signals.

Current	Vibration	Feature Name	Feature Label	Mathematical Expression	Physical Interpretation
I_{mean}	V_{mean}	Mean	F1	$\bar{x} = \frac{1}{N}\sum_{n=1}^{N}[x(n)]$	Kinetic energy related
I_{RMS}	V_{RMS}	RMS	F2	$\sqrt{\frac{1}{N}\sum_{n=1}^{N}[x(n)]^2}$	Kinetic energy related feature
I_{SF}	V_{SF}	Shape Factor	F3	$\frac{\sqrt{\frac{1}{N}\sum_{n=1}^{N}(x(n))^2}}{\frac{1}{N}\sum_{n=1}^{N}\lvert x(n)\rvert}$	Sinusoidal wave shape related
I_{STD}	V_{STD}	Standard Deviation	F4	$\frac{1}{N}\sum_{n=1}^{N}[x(n)-\bar{x}]^2$	Degree of data dispersion
I_{RSSQ}	V_{RSSQ}	Root Sum of Squares	F5	$\sqrt{\sum_{n=1}^{N}[x(n)]^2}$	Kinetic energy related feature
I_{PRMS}	V_{PRMS}	Peak-to-RMS	F6	$\frac{T_{PV}}{T_{RMS}}$	Kinetic energy related feature
I_{CF}	V_{CF}	Crest Factor	F7	$\frac{\max[x(n)]}{RMS}$	Sinusoidal wave shape related
I_{NORM}	V_{NORM}	L2-Norm	F8	$\left[\sum_{i}\lvert x_i\rvert^2\right]^{1/2}$	Degree of data dispersion
I_{RVF}	V_{RVF}	Root Variance Frequency	F9	$\sqrt{\frac{\sum_{n=1}^{N}(f_n - f_{char})^2 x(n)}{\sum_{n=1}^{N}x(n)}}$	Spectral power convergence
I_{ENT}	V_{ENT}	Entropy	F10	$-\sum_{n=1}^{N}\frac{x(n)}{\sum_{k=1}^{N}X_k}log\frac{x(n)}{\sum_{k=1}^{N}X_k}$	Signal Disorientation related
I_{MEAN}	V_{MEAN}	Mean Frequency	F11	$\frac{1}{N}\sum_{k=1}^{N}f_k$	Frequency quantification related
I_{MVI}	V_{MVI}	Moving energy-based index	F12	$\frac{1}{T_s}\sum_{n=1}^{k}x(n)^2$	Signal's energy related

for the postprocessing, vibration feature set is selected for F1 feature.

$$mon = \left|\frac{dF>0}{T-1} - \frac{dF<0}{T-1}\right| \tag{10}$$

Selected features from monotonic trends are further reduced based on correlation. The threshold for independence was set to be 0.50. Features having a correlation score more than 0.50 were eliminated and thus we chose a total of 8 features. In order to have better accuracy in model predictions, selected features were further reduced to a 2-dimentional principal component analysis (PCA) space. Additional scaling or normalization is avoided during the training of the ANN model. Number of hidden layers chosen for the model is 2 where each layer comprises of 512 neurons.

As we chose a large number of neurons, model can get overfitted which is a commonly occurring phenomenon in neural nets. To avoid overfitting, we have used a regularization method named "Dropout", which randomly ignores some output of the previous layer neurons by temporarily removing it from the network. The Dropout rate set for training ANN was 0.15. Several values for different hyperparameters were tested for ANN model. Based on the computational time and accuracy, the best ones are chosen for training. A list of model parameters is presented in Table 4.

70% of the total data were used as the training samples and 15% of these samples were used as validation set to computed validation accuracy during the training stage. The learning curves for 1000 epochs are presented in Fig. 9. It took around 400 epochs for the model to reach to a stable performance

TABLE 4. ANN model parameters.

Parameter	Values
Layer	ANN
Hidden Layers	2
Hidden layer neurons	512, 128
Optimizer	Adam
Dropout	0.15
Loss Function	Categorical crossentropy
Epochs	1000
Activation	Relu
Learning rate	0.0001
Batch size	14

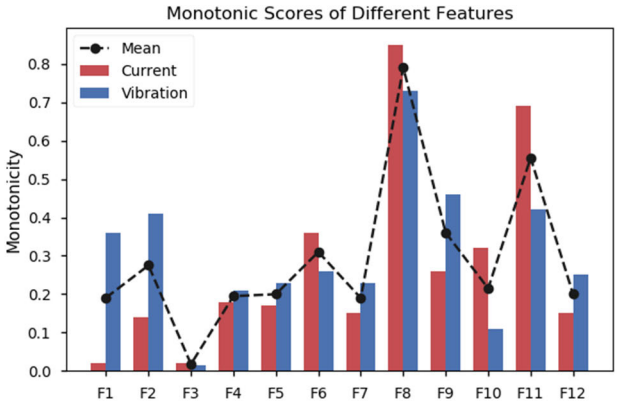

FIGURE 8. Feature selection based on monotonicity.

TABLE 5. Performance metrics of ANN model.

Metrics	Train Set			Test Set		
	Healthy	WSC	CRF	Healthy	WSC	CRF
Precision	0.99	0.97	0.97	0.99	0.96	0.97
Recall	1.00	0.96	0.97	0.99	0.96	0.97
F1-Score	0.99	0.97	0.97	0.99	0.96	0.97

point. To avoid overfitting due to a large number of neurons in the hidden layers, we have used dropout to randomly disable some neurons during the training stages. This allows the model to randomly deactivate some neurons during the forward propagation computation of model training stage. In the output layer, a SoftMax activation function is used that computes the probability of the desired class. After a satisfactory training step, the trained model is used to predict the test data and classify. Among the 1800 healthy label features, 1786 were predicted correctly and 12 were predicted as

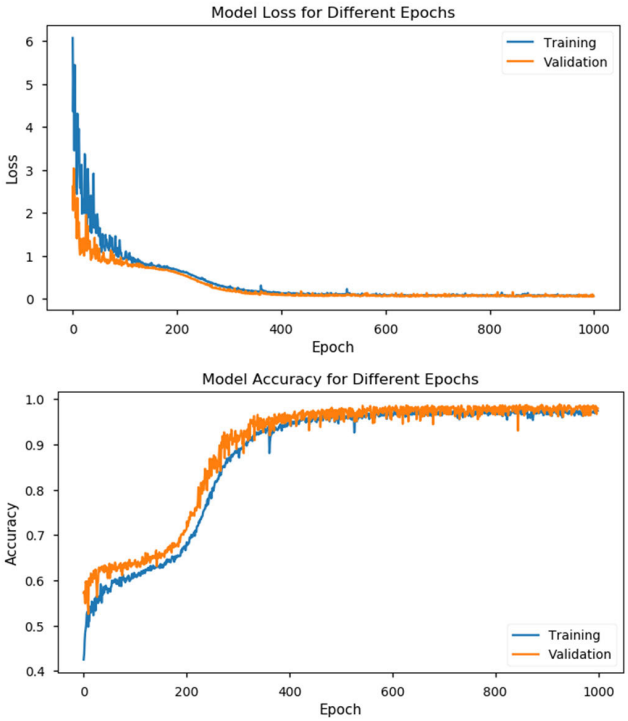

FIGURE 9. ANN model loss and accuracy for different epochs.

WSC fault and 1 as CRF fault. The largest misclassification is seen for WSC fault classification where 1731 were classified accurately, and 11 were predicted as healthy samples and 61 were predicted as CRF fault samples. On the other hand, in case of CRF fault, 1738 samples were predicted accurately, and 57 were predicted as WSC fault samples and 3 as healthy samples. It is understandable that healthy and CRF features are well oriented to be classified separately. However, WSC fault features have some overlapping with healthy and CRF fault features, making some inaccurate predictions in test data. If we look at the confusion matrix of the train data, a similar thing can be observed for WSC fault. This is due to the cyclostationarity behavior of the CRF fault signal. Due to the crack in rotor, each rotation leaves an impulsive on vibration of BLDC motor. These vibration impulses result in larger distortions and abruptly changing frequency responses which are captured as different HIs during feature extraction. To better understand the performance of the ANN model, we have computed several performance metrics based on the predicted values and actual values. Mathematical expressions of the metrics are shown in (11)- (14):

$$Precision = \frac{TP}{TP + FP} \tag{11}$$

$$Recall = \frac{TP}{TP + FN} \tag{12}$$

$$F1 = 2 \times \frac{Precision \times Recall}{Precision + Recall} \tag{13}$$

$$Accuracy = \frac{TP + TN}{TP + TN + FP + FN} \tag{14}$$

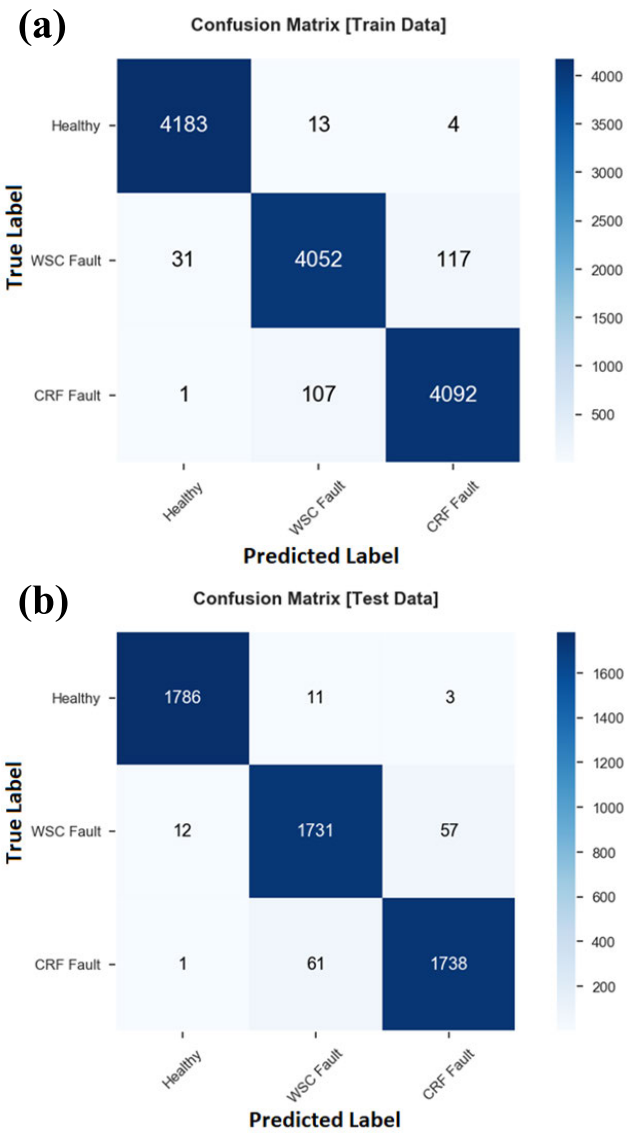

FIGURE 10. Confusion matrix for ANN predictions. (a) Train data, (b) Test data.

where,

TP = True positive
TN = True negative
FP = False positive
FN = False negative

Accuracy indicates the overall performance of the model. For test data set, ANN achieved an accuracy of 98%. As mentioned on Section III, CEEMD is used in this study to decompose the vibration signals into corresponding IMFs. In literature, there are several other mode function decomposition methods such as EMD, EEMD, etc. To better understand the outcome of CEEMD, we have compared the model accuracy for other decomposition methods too. The comparison result is presented in Table 6. CEEMD is a time-consuming algorithm compared to other algorithms due to the adaptive noise addition in each IMF computation. But the ANN accuracy achieved by the CEEMD decomposition

TABLE 6. Performance comparison with other methods.

Decomposition Method	Selected IMF		Accuracy	Time (s)
	Healthy	Faulty		
Raw Signal	-	-	83.3%	-
EMD	IMF-1	IMF-1	91.5%	3
EEMD	IMF-1	IMF-1	94.2%	11
CEEMD	IMF-3	IMF-3	98%	17

outperforms other decomposition techniques. The major contribution of CEEMD technique is that equal distribution of mode functions in each iteration. In the case of EMD and EEMD, the most significant IMF is the IMF-1. EMD fails to capture fault characteristics due to the nonstationary fault characteristics and EEMD causes the IMFs to lose fault information during the reconstructions. CEEMD overcomes these drawbacks by adding an adaptive noise at each stage of IMF computation and hence an improved classification accuracy.

As the commutation is by means of electromagnetic induction, stator coil and rotor are prone to failures in a BLDC motor. Outcomes of this study is the accurate detection and identification of multiple faults in BLDC motor using a single approach, ANN. Using a neural network approach further justifies the robustness of the proposed framework as it can be deployed for a larger amount of data.

VI. CONCLUSION

Fault detection and identification (FDI) is important for a rotary machinery to ensure maximum uptime in industrial applications. Negligence of proper condition monitoring approach can lead to frequent shutdown of the system and gradual decrease in the production. In many cases, a faulty component can cause for catastrophic failures that can be detrimental to humans and environment. This paper presents a fault detection and identification framework considering multiple faults in BLDC motors. Artificial faults were produced in rotor and stator part since these two are the most vital elements of a BLDC motor. Faults were detected by motor current signature analysis where the magnitude and frequency of third harmonic components were computed. Later, hidden fault characteristics were extracted from the vibration and current signals. Vibration signals were decomposed into mode functions to better isolate the fault related information. An improved version of EMD technique, CEEMD is used to decompose the signals and fault features were extracted from a single IMF. Several features were computed from the current and vibration signals, and the most significant ones are selected based on monotonicity, correlation and then

reduced using the PCA. It is found out that CEEMD methods obtains a higher classification accuracy compared to other decomposition techniques. Also, the ANN model was able to successfully classify three different health states with an accuracy of 98%.

In this study we have proposed a fault diagnosis approach of BLDC motor using multi sensor information fusion. This study can be further extended to modeling a degradation trend from healthy state to faulty state using a deep learning regression model. That will allow to estimate the remaining useful life of BLDC motor at a given instance when a fault takes place.

REFERENCES

[1] M. G. Pecht and M. Kang, Eds., *Prognostics and Health Management of Electronics: Fundamentals, Machine Learning, and the Internet of Things*. Hoboken, NJ, USA: Wiley, 2018, pp. 1–136.
[2] J. Lee, F. Wu, W. Zhao, M. Ghaffari, L. Liao, and D. Siegel, "Prognostics and health management design for rotary machinery systems—Reviews, methodology and applications," *Mech. Syst. Signal Process.*, vol. 42, nos. 1–2, pp. 314–334, Jan. 2014.
[3] O. Fink, Q. Wang, M. Svensén, P. Dersin, W.-J. Lee, and M. Ducoffe, "Potential, challenges and future directions for deep learning in prognostics and health management applications," *Eng. Appl. Artif. Intell.*, vol. 92, Jun. 2020, Art. no. 103678.
[4] H. A. Toliyat, *Electric Machines: Modeling, Condition Monitoring, and Fault Diagnosis*. Boca Raton, FL, USA: CRC Press, 2012, pp. 113–187.
[5] J.-W. Hur and T. Alam, "Motor vibration analysis for the fault diagnosis in nonstationary operating conditions," *Int. J. Integr. Eng.*, vol. 12, no. 3, pp. 151–160. [Online]. Available: https://publisher.uthm.edu.my/ojs/index.php/ijie/article/view/5342
[6] S. Choi, E. Pazouki, J. Baek, and H. R. Bahrami, "Iterative condition monitoring and fault diagnosis scheme of electric motor for harsh industrial application," *IEEE Trans. Ind. Electron.*, vol. 62, no. 3, pp. 1760–1769, Mar. 2015.
[7] S.-H. Kim, *Electric Motor Control: DC, AC, and BLDC Motors*. Amsterdam, The Netherlands: Elsevier, 2017, pp. 389–416.
[8] T. A. Shifat and J. W. Hur, "An effective stator fault diagnosis framework of BLDC motor based on vibration and current signals," *IEEE Access*, vol. 8, pp. 106968–106981, 2020, doi: 10.1109/ACCESS.2020.3000856.
[9] J.-K. Park and J. Hur, "Detection of inter-turn and dynamic eccentricity faults using stator current frequency pattern in IPM-type BLDC motors," *IEEE Trans. Ind. Electron.*, vol. 63, no. 3, pp. 1771–1780, Mar. 2016.
[10] J.-K. Park, C.-L. Jeong, S.-T. Lee, and J. Hur, "Early detection technique for stator winding inter-turn fault in BLDC motor using input impedance," *IEEE Trans. Ind. Appl.*, vol. 51, no. 1, pp. 240–247, Jan. 2015.
[11] C. Kar and A. R. Mohanty, "Monitoring gear vibrations through motor current signature analysis and wavelet transform," *Mech. Syst. Signal Process.*, vol. 20, no. 1, pp. 158–187, Jan. 2006.
[12] S. H. Kia, H. Henao, and G.-A. Capolino, "Gear tooth surface damage fault detection using induction machine stator current space vector analysis," *IEEE Trans. Ind. Electron.*, vol. 62, no. 3, pp. 1866–1878, Mar. 2015.
[13] Z. Feng, H. Ma, and M. J. Zuo, "Vibration signal models for fault diagnosis of planet bearings," *J. Sound Vib.*, vol. 370, pp. 372–393, May 2016, doi: 10.1016/j.jsv.2016.01.041.
[14] N. H. Chandra and A. S. Sekhar, "Fault detection in rotor bearing systems using time frequency techniques," *Mech. Syst. Signal Process.*, vols. 72–73, pp. 105–133, May 2016.
[15] D. Wang, K.-L. Tsui, and Q. Miao, "Prognostics and health management: A review of vibration based bearing and gear health indicators," *IEEE Access*, vol. 6, pp. 665–676, 2018.
[16] M. Z. Ali, M. N. S. K. Shabbir, S. M. K. Zaman, and X. Liang, "Single- and multi-fault diagnosis using machine learning for variable frequency drive-fed induction motors," *IEEE Trans. Ind. Appl.*, vol. 56, no. 3, pp. 2324–2337, May 2020.
[17] N. E. Huang, Z. Shen, S. R. Long, M. C. Wu, H. H. Shih, Q. Zheng, N.-C. Yen, C. C. Tung, and H. H. Liu, "The empirical mode decomposition and the Hilbert spectrum for nonlinear and non-stationary time series analysis," *Proc. Roy. Soc. London A, Math., Phys. Eng. Sci.*, vol. 454, no. 1971, pp. 903–995, Mar. 1998.
[18] D. Aggarwal, S. Chandrasekaran, and B. Annamalai, "A complete empirical ensemble mode decomposition and support vector machine-based approach to predict bitcoin prices," *J. Behav. Exp. Finance*, vol. 27, Sep. 2020, Art. no. 100335.
[19] S.-T. Lee and J. Hur, "Detection technique for stator inter-turn faults in BLDC motors based on third-harmonic components of line currents," *IEEE Trans. Ind. Appl.*, vol. 53, no. 1, pp. 143–150, Jan. 2017.
[20] R. Liu, B. Yang, E. Zio, and X. Chen, "Artificial intelligence for fault diagnosis of rotating machinery: A review," *Mech. Syst. Signal Process.*, vol. 108, pp. 33–47, Aug. 2018.
[21] R. Zhao, R. Yan, Z. Chen, K. Mao, P. Wang, and R. X. Gao, "Deep learning and its applications to machine health monitoring," *Mech. Syst. Signal Process.*, vol. 115, pp. 213–237, Jan. 2019, doi: 10.1016/J.YMSSP.2018.05.050.
[22] D. C. Park, M. A. El-Sharkawi, R. J. Marks, L. E. Atlas, and M. J. Damborg, "Electric load forecasting using an artificial neural network," *IEEE Trans. Power Syst.*, vol. 6, no. 2, pp. 442–449, May 1991.
[23] B. Samanta and K. R. Al-Balushi, "Artificial neural network based fault diagnostics of rolling element bearings using time-domain features," *Mech. Syst. Signal Process.*, vol. 17, no. 2, pp. 317–328, Mar. 2003.
[24] Y. Zhang, X. Ding, Y. Liu, and P. J. Griffin, "An artificial neural network approach to transformer fault diagnosis," *IEEE Trans. Power Del.*, vol. 11, no. 4, pp. 1836–1841, Oct. 1996.
[25] J. Ben Ali, N. Fnaiech, L. Saidi, B. Chebel-Morello, and F. Fnaiech, "Application of empirical mode decomposition and artificial neural network for automatic bearing fault diagnosis based on vibration signals," *Appl. Acoust.*, vol. 89, pp. 16–27, Mar. 2015.
[26] T. A. Shifat and J.-W. Hur, "EEMD assisted supervised learning for the fault diagnosis of BLDC motor using vibration signal," *J. Mech. Sci. Technol.*, vol. 34, no. 10, pp. 3981–3990, Oct. 2020, doi: 10.1007/s12206-020-2208-7.
[27] T. Han, Q. Liu, L. Zhang, and A. C. C. Tan, "Fault feature extraction of low speed roller bearing based on Teager energy operator and CEEMD," *Measurement*, vol. 138, pp. 400–408, May 2019.
[28] M. E. Torres, M. A. Colominas, G. Schlotthauer, and P. Flandrin, "A complete ensemble empirical mode decomposition with adaptive noise," in *Proc. IEEE Int. Conf. Acoust., Speech Signal Process. (ICASSP)*, May 2011, pp. 4144–4147.
[29] Y. Yu and C. Junsheng, "A roller bearing fault diagnosis method based on EMD energy entropy and ANN," *J. Sound Vib.*, vol. 294, nos. 1–2, pp. 269–277, Jun. 2006.
[30] N. Saravanan and K. I. Ramachandran, "Incipient gear box fault diagnosis using discrete wavelet transform (DWT) for feature extraction and classification using artificial neural network (ANN)," *Expert Syst. Appl.*, vol. 37, no. 6, pp. 4168–4181, Jun. 2010.
[31] C. Thornton, F. Hutter, H. H. Hoos, and K. Leyton-Brown, "Auto-WEKA: Combined selection and hyperparameter optimization of classification algorithms," in *Proc. 19th ACM SIGKDD Int. Conf. Knowl. Discovery Data Mining*, Aug. 2013, pp. 847–855.
[32] S. Nandi and H. A. Toliyat, "Condition monitoring and fault diagnosis of electrical machines—A review," in *Proc. Conf. Rec. IEEE Ind. Appl. Conf. 34th IAS Annu. Meeting*, vol. 1, Oct. 1999, pp. 197–204.
[33] M. Hamadache, J. H. Jung, J. Park, and B. D. Youn, "A comprehensive review of artificial intelligence-based approaches for rolling element bearing PHM: Shallow and deep learning," *JMST Adv.*, vol. 1, nos. 1–2, pp. 125–151, Jun. 2019.
[34] X. Yan, Y. Liu, and M. Jia, "A feature selection framework-based multiscale morphological analysis algorithm for fault diagnosis of rolling element bearing," *IEEE Access*, vol. 7, pp. 123436–123452, 2019.
[35] Y. Liao and T. A. Lipo, "Effect of saturation third harmonic on the performance of squirrel-cage induction machines," *Electr. Mach. Power Syst.*, vol. 22, no. 2, pp. 155–171, Mar. 1994, doi: 10.1080/07313569408955560.
[36] L. Guo, N. Li, F. Jia, Y. Lei, and J. Lin, "A recurrent neural network based health indicator for remaining useful life prediction of bearings," *Neurocomputing*, vol. 240, pp. 98–109, May 2017.

TANVIR ALAM SHIFAT (Graduate Student Member, IEEE) received the B.Sc. degree in electrical and electronic engineering from East West University, Bangladesh, in 2016. He is currently a Graduate Student with the Department of Aeronautics, Mechanical, and Electronic Convergence Engineering, Kumoh National Institute of Technology. He is also working as a full-time Graduate Research Assistant with the Defense Reliability Laboratory. His research interests include the advanced signal processing and machine learning techniques for the condition monitoring of electric motors. His research interests also include reliability, maintainability, condition monitoring of rotary machinery, electric machines, and so on.

JANG-WOOK HUR received the Ph.D. degree in mechanical engineering from the Tokyo Institute of Technology, Japan, in 1995. He has served for Korean Army from and ranked colonel in 2011. He is currently serving as a Professor for the Department of Aeronautics, Mechanical, and Electronic Convergence Engineering, Kumoh National Institute of Technology. He is also the Director of Defense Reliability Laboratory, Kumoh National Institute of Technology. His research interests include reliability, maintainability, and condition monitoring of various defense equipment.